Supplementary Information

Mass distribution measurements of real samaras

To measure the mass distribution of real samaras, we collected representative samples from various species and scanned their surfaces using a KSCAN-Magic Handheld 3D Scanner (0.02 mm accuracy). By assuming a uniform mass distribution, we calculated the COM for each sample and aligned the samara models such that the COM was positioned at the origin of a coordinate system aligned with the principal axes of inertia. We then identified the geometric center on the plane perpendicular to the axis with the largest moment of inertia, which typically corresponds closely to the samara's surface. Using the modeling files, we measured the maximum extents in two directions within this plane, defining these as the lengths of the longer and shorter edges. These measurements allowed us to calculate the relative COM location for each samara sample using Equation 1-1. The thickness distribution across different samaras is shown in Figure S6, and the corresponding parameters for each are listed in Table S1. Our results show that the mass distributions of the real samaras closely align with those observed in our samara-inspired framework for the corresponding flight modes.

Theoretical model for periodic flight patterns

Among the samara-inspired flight modes discussed, as well as similar behaviors seen in natural samaras, there are two typical periodic modes, i.e. the AR and ST modes. To explore the self-sustaining mechanisms underlying these behaviors, a theoretical model is proposed. Considering the flattened shape of real samaras and the plate model used in our analysis, both reasonably satisfy the relationship $I_3 = I_1 + I_2$, where I_1 and I_2 represent the moments of inertia about the longer and shorter axes, respectively, and I_3 corresponds to the axis perpendicular to the plane of the samara.

Euler's equations of rotation in this context are:

$$I_1\dot{\omega}_1 + I_1\omega_2\omega_3 = M_1 \tag{S1 − 1}$$

$$I_2\dot{\omega}_1 - I_2\omega_1\omega_3 = M_2 \tag{S1 − 2}$$

$$(I_1 + I_2)\dot{\omega}_3 + (I_2 - I_1)\omega_2\omega_3 = M_3 \tag{S1 − 3}$$

The angular velocities under a 3-2-1 Euler angle formulation are:

$$\omega_1 = \dot{\psi} + \dot{\varphi}\sin\theta \tag{S2 − 1}$$

$$\omega_2 = \dot{\varphi}\cos\theta\sin\psi \tag{S2 − 2}$$

$$\omega_3 = \dot{\varphi}\cos\theta\cos\psi \tag{S2 − 3}$$

Projecting torques onto the y-axis of the ground coordinate system yields:

$$M_y = M_2\cos\psi - M_3\sin\psi \tag{S3}$$

In the AR mode, the plate exhibits a steady, axisymmetric rotation during descent. The torque required to sustain rotation arises primarily from gravitational and aerodynamic forces. Based on kinematic measurements (Figure 3), we approximate that $\dot{\varphi}$ and θ remain constant while $\psi \approx 0$, yielding the following torque component along the y-axis:

$$M_y = -I_2\dot{\varphi}^2 \sin\theta \cos\theta \tag{S4}$$

This torque acts in the negative y-direction. The AR motion promotes the formation of attached LEV and RLVs. These vortical structures induce a negative pressure zone near the plate's tip, generating lift that opposes gravity. Consequently, the aerodynamic lift (f_z), along with the gravity (G), generates torque, maintaining uniform rotation during descent (Figure S7A).

The ST mode is characterized by a spiral descent with rapid tumbling, which can be approximated as a precession with uniform angular velocity. Based on kinematic measurements (Figure 3), we assume $\dot{\psi}$, $\dot{\varphi}$, and θ remain constant, yielding the torque component along the y-axis:

$$\begin{aligned} M_y = -I_2\left(\dot{\varphi}\dot{\psi} + \dot{\varphi}^2\sin\theta\right)\cos\theta\,\cos^2\psi + (I_1 + I_2)\dot{\varphi}\dot{\psi}\cos\theta\,\sin^2\psi \\ -(I_2 - I_1)\dot{\varphi}^2\cos^2\theta\,\sin^2\psi\,\cos\psi \end{aligned} \tag{S5}$$

By integrating Equation (S3) over a full tumbling period $T = \frac{2\pi}{<\dot{\psi}>}$, the torque required to sustain rotation, derived from gravitational and aerodynamic forces, yields an average y-component:

$$< M_y > = \frac{1}{T} \cdot \int_{t_0}^{t_0+T} M_y dt = I_1\dot{\varphi}^2\cos\theta\left(\frac{\dot{\psi}}{\dot{\varphi}} - \frac{I_2}{I_1}\sin\theta\right) \tag{S6}$$

For the continuous ST motion shown in Figure 3 (where $\frac{\dot{\psi}}{\dot{\varphi}} \approx 7.5$, $\frac{I_2}{I_1} \approx 8.9$, and $\theta \approx 38.2°$), the torque acts in the positive y-direction on average. This indicates that the combined effects of lift (f_z) and gravity (G) produce a torque (Figure S7B), guiding the plate along a spiral trajectory during continuous tumbling descent.

Figure S1: Reconstruction of chaotic mode trajectory using experimental kinematic data.

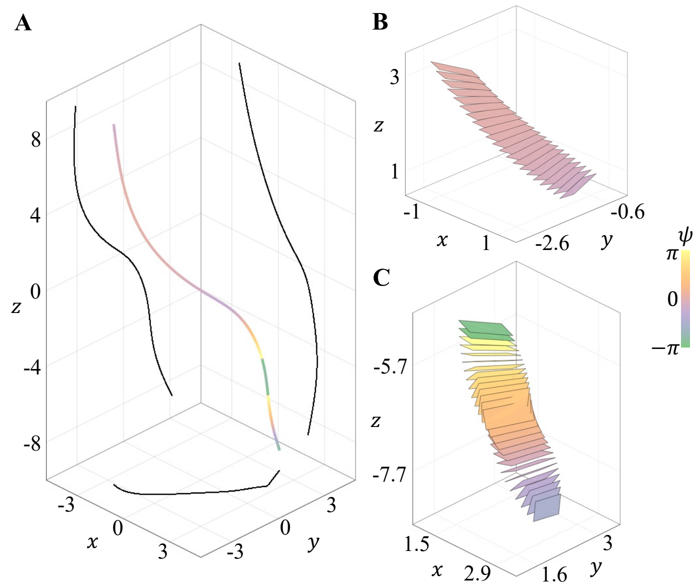

Trajectories of chaotic (CH) flight mode is visualized, with data normalized by the plate's length (L) and reconstructions overlaid at $5ms$ intervals (see also movie S1). **(A)** Overall trajectory. **(B)** 3D reconstruction of the translational-dominated phase. **(C)** 3D reconstruction of the tumbling-dominated phase. 3D reconstructions use the self-rotation angle (ψ) around the plate's longer axis, coloring the plate from green to orange.

Figure S2: Reconstruction of falling mode trajectory using experimental kinematic data.

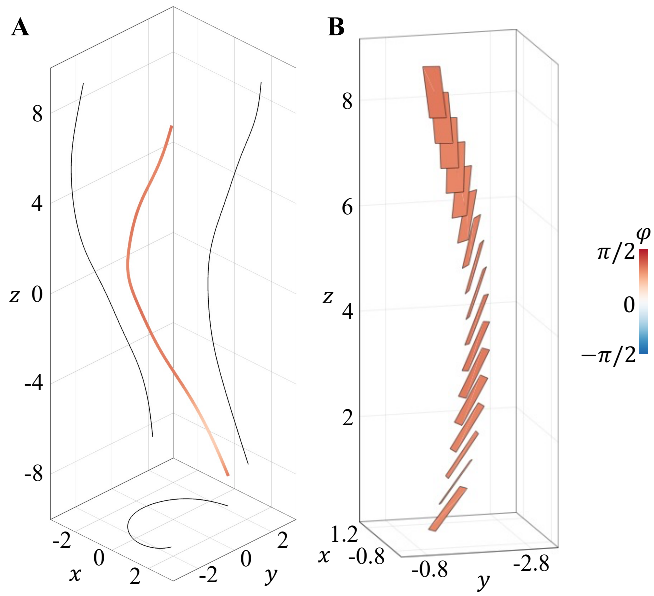

Trajectories of falling (FA) flight mode is visualized, with data normalized by the plate's length (L) and reconstructions overlaid at $15ms$ intervals (see also movie S1). **(A)** Overall trajectory. **(B)** 3D reconstruction of the falling flight mode. 3D reconstructions use the cone angle (θ) between its longer axis and the horizontal plane, coloring the plate from blue to red.

Figure S3: Schematic of experimental platform

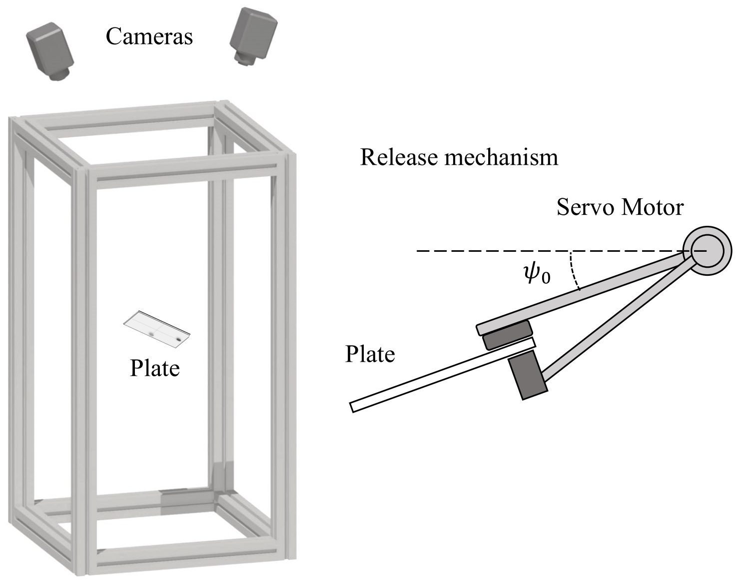

Experiment setup showing the overall arrangement with plate release mechanism.

Figure S4: Simultaneous snapshots of the falling plate

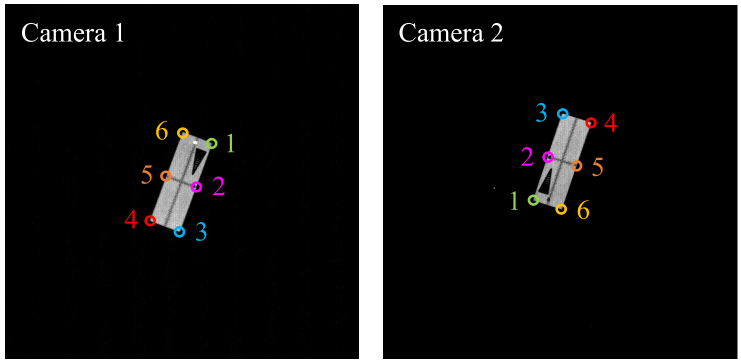

Scatters representing the six reference points on the plate used for kinematic measurements.

Figure S5: Computational fluid dynamics simulation setup

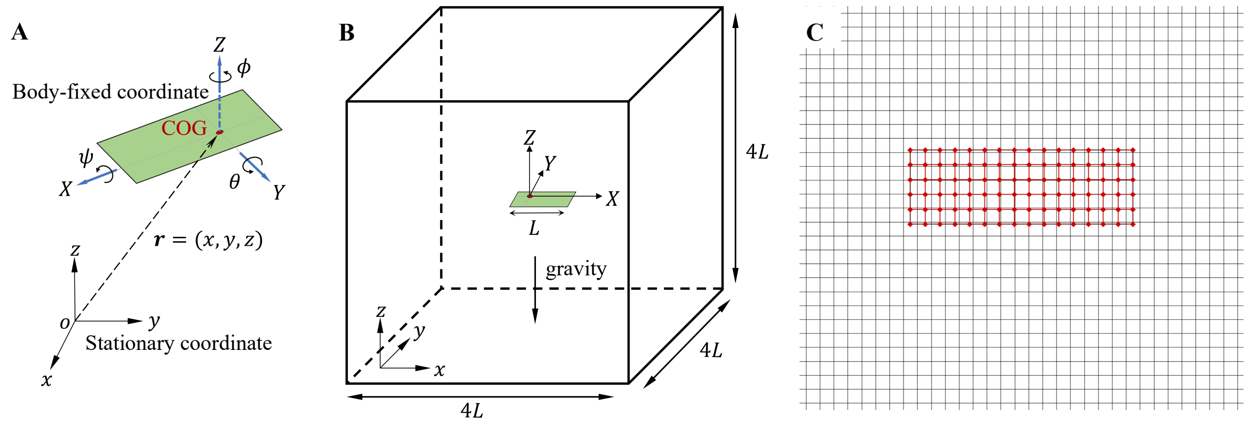

(A) Schematic of coordinate definition. **(B)** Numerical simulation domain. **(C)** Discretization in immersed boundary method: black mesh shows the background Eulerian grid; red mesh shows the Lagrangian grid on the plate.

Figure S6: Mass distribution of real samaras

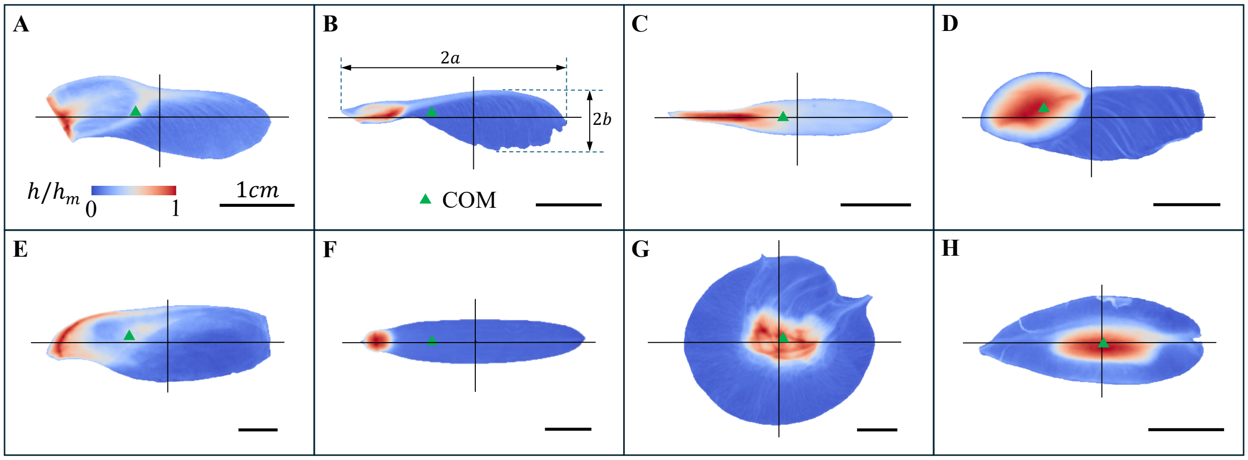

Normalized thickness distributions and center of mass (COM) locations are shown, based on measurements from actual samaras. **(A)** *Acer pictum* (maple), **(B)** *Acer negundo* (maple), **(C)** *Fraxinus* (ash), **(D)** *Pterolobium punctatum*, **(E)** *Swietenia mahagoni* (mahogany), **(F)** *Ventilago leiocarpa*, **(G)** *Pterocarpus santalinus* (red sandalwood), and **(H)** *Eucommia ulmoides*. The green triangles mark the COM locations, while the two orthogonal axes represent the directions parallel to the principal axes of rotational inertia, intersecting at the geometric center of each samara's plane. h/h_m stands for the normalized thickness.

Figure S7: Schematics of self-sustaining mechanism.

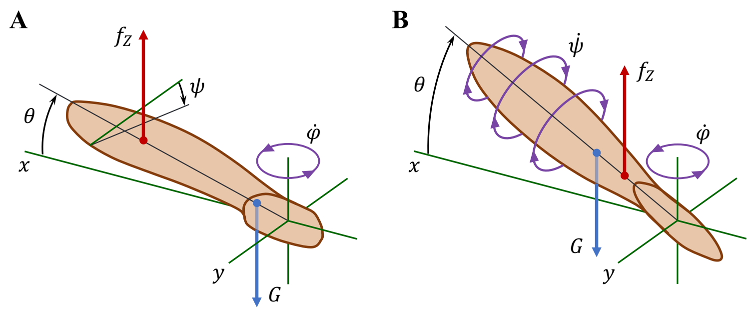

(A) AR mode. **(B)** ST mode. $\dot{\varphi}$ and $\dot{\psi}$ represent the angular velocities around the vertical axis and the plate's longer axis, respectively. Aerodynamic lift (f_z) and gravitational force (G) are also shown.

Table S1 Mass distribution measurements of real samaras

Samaras	x_c/a	y_c/b	$2a\ (mm)$	$2b\ (mm)$	$h_m\ (mm)$	$m_{total}\ (mg)$	Mode
1	0.21	0.12	30.12	11.20	1.78	50.7	AR
2	0.37	0.15	34.32	9.39	2.07	16.6	AR
3	0.12	0.01	32.09	5.45	1.82	33.7	ST
4	0.42	0.19	33.64	13.48	3.55	165.4	AR
5	0.35	0.15	57.93	20.09	2.96	53.8	AR
6	0.38	0.01	49.22	10.19	5.24	83.4	FA
7	0.04	0.04	47.82	43.37	4.27	503.9	ST
8	0.02	0.04	29.94	11.98	2.01	78.7	ST

This table summarizes the key parameters from the measurements of real samaras, including their morphological and mass distribution properties. x_c/a and y_c/b denote the relative coordinates of the COM along the x and y directions, respectively, with $2a$ and $2b$ representing the maximum extents in those directions within the samara plane. h_m stands for the maximum thickness, and m_{total} indicates the total mass of each samara. The corresponding flight modes are listed alongside these parameters. Images and detailed mass distribution of these samaras are shown in Figure 1A and Figure S6, respectively.

Movie S1.

3D reconstruction of flight modes in the samara-inspired framework

Movie S2.

Visualization of vortical structures in samara-inspired flight